

1 **Aerosol transport pathways and source attribution in China**
2 **during the COVID-19 outbreak**

3

4

5 Lili Ren¹, Yang Yang^{1*}, Hailong Wang², Pinya Wang¹, Lei Chen¹, Jia

6 Zhu¹, Hong Liao¹

7

8

9

10

11 ¹Jiangsu Key Laboratory of Atmospheric Environment Monitoring and Pollution
12 Control, Jiangsu Collaborative Innovation Center of Atmospheric Environment and
13 Equipment Technology, School of Environmental Science and Engineering, Nanjing
14 University of Information Science and Technology, Nanjing, Jiangsu, China

15 ²Atmospheric Sciences and Global Change Division, Pacific Northwest National
16 Laboratory, Richland, Washington, USA

17

18

19

20

21 *Correspondence to yang.yang@nuist.edu.cn

22

23 Abstract

24 Due to the coronavirus disease 2019 (COVID-19) pandemic, human
25 activities and industrial productions were strictly restricted during January-
26 March 2020 in China. Despite the fact that anthropogenic aerosol
27 emissions largely decreased, haze events still occurred. Characterization of
28 aerosol transport pathways and attribution of aerosol sources from specific
29 regions are beneficial to the air quality and pandemic control strategies.
30 This study establishes source-receptor relationships in various regions
31 [covering the whole](#) China during the COVID-19 outbreak based on the
32 Community Atmosphere Model version 5 with Explicit Aerosol Source
33 Tagging (CAM5-EAST). Our analysis shows that PM_{2.5} burden over the
34 North China Plain between January 30 and February 19 is [largely mostly](#)
35 contributed by local emissions (40–66%). For other regions in China, PM_{2.5}
36 burden is largely contributed from non-local sources. During the [most](#)
37 polluted days of COVID-19 outbreak, local emissions within North China
38 Plain and Eastern China, respectively, contribute 66% and 87% to the
39 increase in surface PM_{2.5} concentrations. This is associated with the
40 anomalous mid-tropospheric high pressure at the location of climatological
41 East Asia trough and the consequently weakened winds in the lower
42 troposphere, leading to the local aerosol accumulation. The emissions
43 outside China, especially [those](#) from South and Southeast Asia, contribute
44 over 50% to the increase in PM_{2.5} concentration in Southwestern China

45 through transboundary transport during the [most](#) polluted day. As the
46 reduction in emissions in the near future, aerosols from long-range
47 transport together with unfavorable meteorological conditions are
48 increasingly important to regional air quality and need to be taken into
49 account in clean air plans.

50 1. Introduction

51 The coronavirus disease 2019 (COVID-19) ~~had an outbreak in China~~
52 ~~in~~ has spread worldwide since December 2019. ~~It has~~ and resulted in more
53 than one million cases within the first four months ~~worldwide~~ (Sharma et
54 al., 2020; Dong et al., 2020). In order to curb the virus spread among
55 humans, ~~China was the first country to take dramatic~~ measures were taken
56 by the Chinese government on January 23, 2020 to minimize the
57 interaction among people, including strict isolation, prohibition of large-
58 scale private and public gatherings, restriction of private and public
59 transportation and even lockdown of cities (Tian et al., 2020; Wang et al.,
60 2020). The estimated NO_x emission in eastern China was reduced by 60-
61 70%, of which 70-80% was related to the reduced road traffic and 20-25%
62 was from industrial enterprises shutdown during the COVID-19 lockdown
63 period ~~(Huang et al., 2020)~~. However, severe air pollution events still
64 occurred in East China during the COVID-19 lockdown. ~~It is of great~~
65 ~~concern that why severe air pollution was not avoided by decreasing, even~~
66 though the anthropogenic emissions were greatly reduced (Huang et al.,
67 2020). The unprecedented large-scale restrictions resulting from the
68 COVID-19 epidemic provide an opportunity to research the relationship
69 between dramatic anthropogenic emission reductions and air quality
70 ~~change~~ changes (e.g., Bao et al., 2020; Li et al., 2020; Wang et al., 2020).
71 Bao et al. (2020) reported that, during the COVID-19 lockdown period, the

72 air quality index (AQI) and the PM_{2.5} (particulate matter less than 2.5 μm
73 in diameter) concentration were decreased by 7.8% and 5.9 %, respectively,
74 on average in 44 cities in northern China, mainly due to travel restrictions.
75 By applying the WRF-CAMx model together with air quality monitoring
76 data, Li et al. (2020) revealed that although primary particle emissions were
77 reduced by 15%–61% during the COVID-19 lockdown over the Yangtze
78 River Delta Region, the daily mean concentration of PM_{2.5} was still
79 relatively high, reaching up to 79 μg m⁻³. Wang et al. (2020) found that the
80 relative reduction in PM_{2.5} precursors was twice as much as the reduction
81 in PM_{2.5} concentration, in part due to the unfavorable meteorological
82 conditions during the COVID-19 outbreak in China that led to the
83 formation of the heavy haze. Huang et al. (2020) and Le et al. (2020)
84 reported that stagnant air conditions, high atmospheric humidity, and
85 enhanced atmospheric oxidizing capacity led to a severe haze event in
86 northern China during the COVID-19 pandemic.

87 Aerosols are main air pollutants that play important roles in the
88 atmosphere due to their adverse effects on air quality, visibility (Vautard et
89 al., 2009; Watson, 2002), human health (Lelieveld et al., 2019; Heft-Neal
90 et al., 2018), the Earth's energy balance, and regional and global climate
91 (Ramanathan et al., 2001; Anderson et al., 2003; Wang et al., 2020; Smith
92 et al., 2020). With the rapid development in recent decades, China has
93 experienced severe air pollutions that damage human health and cause

94 regional climate change (Chai et al., 2014; Liao et al., 2015; Fan et al.,
95 2020). In order to control air pollution, the Chinese government issued and
96 implemented the Air Pollution Prevention and Control Action Plan in 2013
97 (China State Council, 2013). Although emissions in China have decreased
98 significantly in recent years (Zheng et al., 2018), aerosols transported from
99 other source regions could add on top of local emissions (Yang et al., 2017a,
100 2018a; Ren et al., 2020). Therefore, it is important to understand the
101 relative effects of local emissions and regional transport on aerosols in
102 China.

103 Source tagging and apportionment is an effective way to establish
104 aerosol source-receptor relationships, which is conducive to both scientific
105 research and emission control strategies (Yu et al., 2012). By applying the
106 Particulate Source Apportionment Technology in CAMx model, Xue et al.
107 (2014) found that the contributions of regional transport to annual average
108 PM_{2.5} concentrations in Hainan, Shanghai, Jiangsu, Zhejiang, Jilin and
109 Jiangxi provinces of China are more than 45%. By adding a chemical tracer
110 into the WRF model, Wang et al. (2016) studied the sources of black carbon
111 (BC) aerosol in Beijing and reported that about half of BC in Beijing came
112 from the central North China Plain. Liu et al. (2017) applied WRF-Chem
113 model and showed that Foshan, Guangzhou and Dongguan, respectively,
114 with relatively high emissions contributed 14%, 13% and 10% to the
115 regional mean PM_{2.5} concentration in the Pearl River Delta.

116 Currently, ~~many previous studies only focused on regional transport of~~
117 ~~aerosols, very few~~ studies have ~~investigated the impact of reduced human~~
118 ~~activity on regional air quality, as a result of the COVID-19 outbreak. Few~~
119 ~~studies have focused on~~ explored the aerosol transport pathways and source
120 attribution ~~in~~ covering the whole China during the COVID-19 pandemic. In
121 this study, the global aerosol-climate model CAM5 (Community
122 Atmosphere Model, version 5) equipped with an Explicit Aerosol Source
123 Tagging (CAM5-EAST) is employed to quantify source-receptor
124 relationships and transport pathways of aerosols during the COVID-19
125 outbreak in China. We also provide model evaluations of PM_{2.5}
126 concentrations against observations made during the COVID-19 outbreak.
127 With the aerosol source tagging technique, source region contributions to
128 PM_{2.5} column burden over various receptor regions and transport pathways
129 in China are analyzed. The source contributions to the changes in near-
130 surface PM_{2.5} in ~~the most~~ polluted days compared to the monthly means
131 during February 2020 are also quantified. ~~This paper~~ Our study provides
132 source apportionment of aerosols ~~in~~ covering the whole China ~~during~~
133 ~~the~~ and quantifies the contribution from foreign transport for the first time
134 ~~in the case of~~ COVID-19 emission reductions, which is beneficial to the
135 investigation of policy implications for future air pollution control.

136 **2. Methods**

137 **2.1 Model description and experimental setup**

138 The CAM5 model is applied to estimate the PM_{2.5} changes during the
139 COVID-19 period. ~~In CAM5~~, which is the atmospheric component of the
140 earth system model CESM (Community Earth System Model, Hurrell et
141 al., 2013). In this study, major aerosol species including sulfate, BC,
142 primary organic matter (POM), secondary organic aerosol (SOA), sea salt,
143 and mineral dust, are represented by three lognormal size modes (i.e.,
144 Aitken, accumulation, and coarse modes) of the modal aerosol module
145 (MAM3) (Liu et al., 2012). The detailed aerosol representation in CAM5
146 was provided in Liu et al. (2012) and Wang et al. (2013). The aerosol
147 mixing states consider both internal mixed (within a same mode) and
148 external mixed (between modes). On top of the default CAM5, additional
149 modifications that improve the representation of aerosol wet scavenging
150 and convective transport (Wang et al., 2013) are also included in the model
151 version used for this study.

152 In this study, simulations were conducted with a horizontal resolution
153 of $1.9^\circ \times 2.5^\circ$ and 30 vertical layers up to 3.6 hPa in year 2020.
154 ~~Anthropogenic~~The anthropogenic emissions used in Chinathe baseline
155 simulation are derived from the MEIC (Multi-resolution Emission
156 Inventory of China) inventory (Zheng et al., 2018)~~), while~~, referred to here
157 as the Baseline experiment. While emissions for the other countries use the
158 SSP (Shared Socioeconomic Pathways) 2–4.5 scenario data set under
159 CMIP6 (the Coupled Model Intercomparison Project Phase 6). Emissions

160 in year 2017 are used as the baseline during the simulation period
161 considering the time limit of MEIC inventory. To better estimate the impact
162 of restricted human activities on emission reductions owing to COVID-19
163 lockdown, (referred to as Covid experiment), we updated China's emission
164 inventory from January to March 2020 based on the provincial total
165 emission reduction ratio in Huang et al. (2020). Emissions from the
166 transportation sector are decreased by 70% ~~and the~~%. The remaining
167 reduction emission reduction, by excluding transport reduction from the
168 total emission reduction, are evenly distributed to other sectors, including
169 industry, power plant, residential, international shipping and waste
170 treatment from January to March 2020 compared to the baseline emission
171 in 2017. Unless otherwise specified, all the results in this study are derived
172 from the Covid experiment.

173 The sea surface temperature, sea ice concentrations, solar radiation and
174 greenhouse gas concentrations are fixed at present-day climatological
175 levels. To capture the large-scale atmospheric circulations during the
176 COVID-19, we nudge the model wind fields toward the MERRA-2
177 (Modern-Era Retrospective Analysis for Research and Applications,
178 version 2) reanalysis (Gelaro et al., 2017) from April 2019 to March 2020
179 repeatedly for six years. Only model results from the last year are used to
180 represent year 2020. with the first five years as model spin-up. In this study,
181 we analyze the transport pathways and source attribution of aerosols during

182 the three weeks that had the largest number of newly-diagnosed COVID-
183 19 cases (Fig. [2S1](#), hereafter referred to as the ‘Week 1’: January 30–
184 February 5, ‘Week 2’: February 6–February 12 and ‘Week 3’: February 13–
185 February 19), when unexpected hazardous air pollution events also
186 occurred during this time period ([Huang et al., 2020](#); [Le et al., 2020](#)).

187 **2.2 Explicit aerosol source tagging and source regions**

188 To examine the source apportionment of aerosols in China, the Explicit
189 Aerosol Source Tagging (EAST) technique was implemented in CAM5,
190 which has been utilized in many aerosol source attribution studies (e.g.,
191 Wang et al., 2014; Yang et al., 2017a, b, 2018a, b, c, 2020; Ren et al., 2020).
192 Different from the emission sensitivity method that assumes a linear
193 response to emission perturbation and the traditional backward trajectory
194 method, aerosols from each tagged region or sector are calculated
195 independently in EAST within one single simulation. Without relying on a
196 set of model simulations with emission perturbations or assuming constant
197 decaying rate, EAST is more accurate and time-saving than the source
198 apportionment method mentioned above. In addition to the sulfate, BC and
199 POM species that were tagged in previous studies (e.g., Yang et al., 2020),
200 SOA and precursor gas are now also tagged in the EAST. These types of
201 aerosols from independent source regions and sectors can be explicitly
202 tagged and tracked simultaneously. In this study, focusing on the aerosols
203 in China during the COVID-19 outbreak period, the domestic aerosol and

204 precursor emissions ~~are divided into~~from eight geographical source regions
205 (Fig. 1), including Northeastern China (NEC), North China Plain (NCP),
206 Eastern China (ESC), Southern China (STC), Central-West China (CWC),
207 Southwestern China (SWC), Northwestern China (NWC) and the
208 Himalayas and Tibetan Plateau (HTP), and the rest of the world (ROW)
209 emissions), are tagged separately.

210 **3. Model evaluation**

211 Many previous studies have assessed the spatial distribution and
212 seasonal to decadal variations in aerosol concentrations in China and
213 worldwide simulated by CAM5 with the observations (e.g., Wang et al.,
214 2013; Yang et al., 2017a,b, 2018b,c, 2020). In order to evaluate the model's
215 performance in simulating aerosols during the COVID-19 outbreak period
216 in China, the surface concentrations of PM_{2.5}, estimated as the sum of
217 sulfate, BC, POM and SOA for model results, during the analyzed time
218 periods are compared with measurements from the China National
219 Environmental Monitoring Center (CNEMC), as shown in Fig. [3a2a](#). The
220 model reasonably reproduces the overall spatial distribution of near-
221 surface PM_{2.5} concentrations during the three time periods, with high
222 values in the North China Plain and low values in western China. However,
223 as reported in many CAM5 model studies (e.g., Yang et al., 2017a,b), the
224 model underestimates the PM_{2.5} concentrations with normalized mean
225 biases (NMB) of -55%~-49%, compared to the available site observations

226 (Fig. [S1S2](#)). The discrepancies are related to coarse-resolution model
227 sampling bias relative to the observational sites, uncertainties in aerosol
228 emissions, wet removal, and gas-particle exchange. In addition, the model
229 version used in this study is not able to simulate nitrate and ammonium
230 aerosols, which are also the main components of PM_{2.5} (Kong et al., 2020;
231 Xu et al., 2019).

232 The long-distance transport of aerosols mainly occurs in the upper
233 troposphere rather than near the surface (Hadley et al., 2007; Zhang et al.,
234 2015). Aerosols are lifted from the atmospheric boundary layer of the
235 emission source regions to the free troposphere and then undergo the
236 transboundary and intercontinental transport effectively driven by the
237 upper tropospheric circulations. Therefore, it is helpful to analyze the
238 relative contributions of local and non-local sources by focusing on the
239 column burden of aerosols. Figure [3b2b](#) presents spatial distributions of
240 simulated mean column burden of PM_{2.5} during the three time periods:
241 [‘Week 1’: January 30–February 5, ‘Week 2’: February 6–February 12 and](#)
242 [‘Week 3’: February 13–February 19\), which had the largest number of](#)
243 [newly-diagnosed COVID-19 cases](#). The contrast in column burden does
244 not differ significantly from that of near-surface concentrations. [Among the](#)
245 [three time periods](#) [Comparing to Week 3](#), Week 1 and Week 2 have higher
246 PM_{2.5} loading, with values in the range of 20–40 and 20–30 mg m⁻² in the
247 North China Plain, Eastern China, and Southern China, while the PM_{2.5}

248 loading in Week 3 is relative lower with [than Week 1 and Week 2 with](#)
249 values ranging mostly from 10 to 20 mg m⁻². Note that the column burden
250 of PM_{2.5} in South and Southeast Asia is higher than 20 mg m⁻² in three time
251 periods and reaches up to 50 mg m⁻² in Week 2, which potentially
252 influences aerosol concentrations in China through transboundary
253 transport.

254 **4. Transport Pathways**

255 The explicit aerosol tagging technique can clearly identify the transport
256 pathways of aerosols moving from their source regions to their destination.

257 Figure [43](#) shows the spatial distribution of mean column burden of
258 simulated PM_{2.5} originating from the six tagged source regions in central
259 and eastern China and outside of China during the three time periods.
260 Aerosols and/or precursor gases emitted from the various regions follow
261 quite different transport pathways determined by their source locations,
262 meteorological conditions, emission injection height, and physical and
263 chemical characteristics of aerosol species. Aerosols from Northeastern
264 China are transported southeastward by the northwesterly winds (Fig. 1b).
265 From the North China Plain, aerosols can be transported either southward
266 reaching Eastern, Southern and Southwestern China during Week 1 or
267 across east coast of China to the oceanic region during Week 2-3. Aerosols
268 originating from Eastern China move straight to Southwestern and
269 Southern China during Week 1-2, while they also entered the North China

270 Plain during Week 2-3. Aerosols emitted from Southern China and Central-
271 West China have no obvious transport due to their relatively weak
272 emissions. In addition to the local impact, emissions from Southwestern
273 China affect mostly the Southern China and Eastern China. Air parcels with
274 high levels of $PM_{2.5}$ from South and Southeast Asia moved into
275 Southwestern, Southern and Eastern China and even the North China Plain
276 during the three time periods.

277 The vertical distributions of $PM_{2.5}$ emitted from six major tagged
278 source regions are shown in Figs. [S2S3](#) and [S3S4](#). The $PM_{2.5}$ has much
279 higher concentrations in the lower troposphere and decreases with
280 increasing height. During Week 1-2, owing to the presence of high $PM_{2.5}$
281 loadings, a stronger vertical mixing and transport brought more $PM_{2.5}$ to
282 the upper troposphere compared to that during Week 3. High
283 concentrations of $PM_{2.5}$ originating from the North China Plain extended
284 southeastward by strong northwesterly winds. Weak winds over Eastern
285 China led to accumulations of $PM_{2.5}$ within this region, which is consistent
286 with the findings in Yang et al. (2017a). Strong southwesterly winds in the
287 south of Southwestern China and weak winds in the north of this region
288 produced convergences and updrafts that lift aerosols up to 700 hPa.

289 Considering that the emissions outside China contribute greatly to
290 $PM_{2.5}$ concentrations in Southwestern China through transboundary
291 transport (Yang et al., 2017a) and aerosols from East Asia can be

292 transported to the North Pacific and even North America (Yu et al., 2008;
293 Yang et al., 2018c), it is of great importance to study the inflow and outflow
294 of PM_{2.5} across the boundaries of China. Figures 54 and 65 show the
295 vertical distribution of PM_{2.5} concentrations resulting from emissions
296 within and outside China over 29°N, 88°E and 21°N around the south
297 boundaries (cross-sections (CS) 1-3 in Fig. 1a) and 123° E around the east
298 boundary (CS 4 in Fig. 1a) of the mainland of China. Over the southern
299 border, PM_{2.5} concentrations are more influenced by transboundary
300 transport of aerosols from ROW than those originating from domestic
301 emissions. The high concentrations of PM_{2.5} from South and Southeast
302 Asia are lifted into the free atmosphere of the Tibetan Plateau and Yun-Gui
303 Plateau, and then transported to Southern and Southwestern China by
304 southwesterly winds. Over the North China Plain and Eastern China,
305 northwesterly winds at 35-45° N and southwesterly winds at 25-35° N
306 cause aerosols to accumulate in the lower atmosphere and then export
307 across east border of China below 700 hPa.

308 **5. Source apportionment of PM_{2.5} in China during the COVID-19**

309 **5.1 Source contributions to PM_{2.5} burden**

310 Figure 76 shows the simulated relative contributions in percentage to
311 PM_{2.5} column burden from local source emissions, regional transport from
312 the untagged regions of China (rest of China, RCN) and rest of the world
313 (ROW). Over the North China Plain, where emissions are relatively high,

314 PM_{2.5} column burden is dominated by local emissions during the three time
315 periods. In contrast, regions with relative low emissions are mainly
316 affected by nonlocal sources, especially by foreign contributions.
317 Emissions from the ROW contribute a large amount to PM_{2.5} burden over
318 Northeastern, Southern, Central-West, Southwestern, Northwestern China
319 and the Tibetan Plateau. PM_{2.5} burden in Eastern China is greatly
320 contributed by the sources from RCN, especially in Week 1 when regional
321 transport of PM_{2.5} from the North China Plain is relatively strong (Fig.
322 [S3S4](#)).

323 Table 1 summarizes the contributions of tagged source regions to the
324 PM_{2.5} burden over different receptor regions in China. In Northeastern
325 China, 36%-43% of the PM_{2.5} column burden comes from local emissions,
326 while a larger portion (39%-54%) is contributed by emissions from ROW
327 during the three time periods. The impacts of nonlocal sources within
328 China on PM_{2.5} burden are relatively low in Northeastern China during
329 Week 1 with the contribution of less than 5%, while RCN is responsible for
330 23% and 25% during Week 2 and Week 3, respectively.

331 In the North China Plain, the majority of the PM_{2.5} burden is attributed
332 to local emissions in all cases, with local contributions in a range of 40–
333 66%. Emissions from the North China Plain also produce a widespread
334 impact on PM_{2.5} over its neighboring regions. The sources from North
335 China Plain account for 14–33% of the PM_{2.5} burden in Eastern China and

336 7–23% in Southern China during the three time periods.

337 In Eastern China, local emissions account for 27–40% of PM_{2.5} column
338 burden, while ROW contributes 20–45%. Southern China and Central-
339 West China have 13–18% and 25–31% of local source contributions,
340 respectively, whereas 37–64% are due to emissions from outside China in
341 these two regions. In Southwestern China, 15–18% of the PM_{2.5} burden
342 originates from local emissions and 7–24% is from RCN. ROW emissions
343 play important roles in affecting PM_{2.5} burden over this region, with
344 relative contributions in a range of 59–78% during the three time periods,
345 which is associated with the transboundary transport by southwesterly
346 winds. PM_{2.5} burden over the Northwestern China and Himalayas and
347 Tibetan Plateau with relatively low local emissions are strongly influenced
348 by nonlocal sources, where more than 70% of the PM_{2.5} burden originates
349 from emissions outside China.

350 **5.2 Aerosol source attribution during polluted days**

351 In spite of the large reductions in emissions, severe air pollution events
352 still occurred in China during the COVID-19 lockdown. Source attribution
353 of PM_{2.5} during polluted days in China has policy implications for future
354 air pollution control. In Beijing, capital of China over the North China
355 Plain, a serious haze event happened from February 11 to 13, 2020 during
356 the COVID-19 outbreak period according to observations released by
357 CNEMC. CAM5-EAST reproduced the polluted day on February 11 over

358 the North China Plain. In this study, the most polluted day is defined as the
359 day with the highest daily PM_{2.5} concentration in February 2020 for each
360 receptor region in China. Figure 87 presents the composite differences in
361 near-surface PM_{2.5} concentrations and 850 hPa wind fields between [the](#)
362 [most](#) polluted [daysday](#) and normal days (all days in February 2020) for
363 each receptor region. The local and nonlocal source contributions to the
364 PM_{2.5} differences are summarized in Fig. 98.

365 Unexpectedly, near-surface PM_{2.5} concentrations in the North China
366 Plain and Eastern China experienced remarkable increases during the [same](#)
367 [most](#) polluted [daysday](#) of COVID-19 lockdown. The simulated PM_{2.5}
368 concentrations increased, with the largest increases of more than 20 µg m⁻³
369 in the North China Plain and Eastern China, 10 µg m⁻³ maximum increase
370 in the Southwestern China and 5 µg m⁻³ in the Northeastern, Southern and
371 Central-West China, during the most polluted days compared to the normal
372 days.

373 The increase in near-surface PM_{2.5} concentrations during the most
374 polluted day over Northeastern China is largely influenced by the local
375 emissions, which contribute to a regional averaged concentration increase
376 of 1.1 µg m⁻³. This is mainly due to the accumulation of local aerosols
377 under the weakened prevailing northwesterly winds over this region.

378 When the PM_{2.5} pollution occurred in the North China Plain, [on](#)
379 [February 11, 2020, which was also reported as the polluted day in](#)

380 [observations \(Huang et al., 2020\)](#), the concentration of PM_{2.5} was 16.1 μg
381 m⁻³ higher than that in normal days. The contribution from local emissions
382 accounts for 66% of the averaged increase, which was related to the
383 stagnant air condition (i.e., weakened lower tropospheric winds) resulting
384 from the anomalous mid-tropospheric high pressure located at the
385 climatological location of the East Asia trough (Fig. [S4S5](#)). Sources from
386 Eastern China also explain 4.3 μg m⁻³ (27%) of the total increase over the
387 North China Plain.

388 During the most polluted day in Eastern China (the same day as the
389 [most](#) polluted day in North China Plain), the ~~regional averaged increase in~~
390 ~~concentration of~~ PM_{2.5} ~~concentrations is was~~ 16 μg m⁻³ [higher than that in](#)
391 [normal days](#), which is primarily contributed by the local emissions. While
392 the contribution from the North China Plain decreased in the [most](#) polluted
393 day, the anomalous southerly winds brought more aerosols from Southern
394 China and ROW into Eastern China, contributing to 4% and 10% aerosol
395 increase, respectively.

396 Owing to the enhanced northerly winds, emissions from the North
397 China Plain and Eastern China contribute 33% and 39% of the increase,
398 respectively, in PM_{2.5} concentration over Southern China. The most
399 polluted day in Central-West China is mostly caused by local emissions
400 (65% of the total increase).

401 When Southwestern China was under the polluted condition, PM_{2.5}

402 concentration ~~was~~ increased by $2.1 \mu\text{g m}^{-3}$. Emissions from ROW,
403 especially those from South and Southeast Asia, are of great significance
404 to the increase of $\text{PM}_{2.5}$ concentrations due to the enhanced southwesterly
405 winds over this region. The relative contribution from ROW emissions is
406 more than 50% over Southwestern China during the most polluted day. It
407 highlights that the important role of transboundary transport needs to be
408 considered when controlling local emissions to improve air quality in the
409 near future.

410

411 **6. Conclusions and discussions**

412 The COVID-19 pandemic disrupted human activities and lead to abrupt
413 reductions in anthropogenic emissions. This study first investigated the
414 source contributions to $\text{PM}_{2.5}$ over various regions covering the whole
415 China during the COVID-19 pandemic. We pay attention not only to local
416 emissions, but also to the impacts from regional and foreign transport of
417 aerosols. An explicit aerosol source tagging is implemented in the
418 Community Atmosphere Model version 5 (CAM5-EAST) to examine the
419 aerosol transport pathways and source attribution of $\text{PM}_{2.5}$ in China during
420 the first few weeks of the COVID-19 outbreak (Week 1: January 30–
421 February 5, Week 2: February 6–February 12 and Week 3: February 13–
422 February 19). The contributions of emissions to $\text{PM}_{2.5}$ originating from
423 eight source regions in the mainland of China, including Northeastern

424 China, North China Plain, Eastern China, Southern China, Central-West
425 China, Southwestern China, Northwestern China and Himalayas and
426 Tibetan Plateau, and sources outside China (ROW) to near-surface
427 concentrations, column burdens, transport pathways of PM_{2.5}, and haze
428 formation in different receptor regions in China are quantified in this study.

429 Aerosols emitted from the North China Plain, where the air quality is
430 often poor, can be transported through Eastern China and reach
431 Southwestern China during the three time periods. Similarly, aerosols from
432 Eastern China move straight to Southern China and Southwestern China
433 during Week 1 and Week 2, and a significant portion can also enter the
434 North China Plain during Week 2 and Week 3.

435 Across the southern boundary of the mainland of China, high
436 concentrations of PM_{2.5} from South and Southeast Asia are lifted into the
437 free atmosphere and then transported to Southern and Southwestern China.
438 While PM_{2.5} from the North China Plain and Eastern China can also be
439 brought out of China via westerly winds, mostly below 700 hPa.

440 PM_{2.5} in China is affected not only by local emissions but also by long-
441 range transport of pollutants from distant source regions. Over the North
442 China Plain, 40–66% of the PM_{2.5} burden is attributed to local emissions
443 during the COVID-19 outbreak. They also impact PM_{2.5} in neighboring
444 regions, accounting for 14–33% of the PM_{2.5} burden in Eastern China and
445 7–23% in Southern China during the three time periods. Northeastern

446 China has 36%-43% of local source contributions to its PM_{2.5} column
447 burden, while 39%-54% is contributed by emissions from ROW during the
448 three time periods. In Eastern China, local emissions explain 27–40% of
449 PM_{2.5} burden, while ROW contributes 20–45%. In Southwestern China,
450 59–78% of the PM_{2.5} burden is contributed by emissions from ROW. Over
451 the Northwestern China and Himalayas and Tibetan Plateau, ROW
452 emissions have a great contribution of more than 70% to the PM_{2.5} column
453 burden.

454 In this study, the most polluted day is defined as the day with the
455 highest daily PM_{2.5} concentration in February 2020 for each receptor
456 region in China. The transport from outside of China only has a great
457 impact on some specific regions in China. In Southwestern China, the
458 relative contribution from ROW emissions, especially those from South
459 and Southeast Asia, to the increment of PM_{2.5} concentration during the
460 most polluted days compared with normal days is more than 50%. It is
461 consistent with the previous studies that emissions from South and
462 Southeast Asia have an important impact on air quality in southwest China
463 (Yang et al., 2017a; Zhu et al., 2016, 2017). For other receptor regions in
464 China (Northeastern China, North China Plain, Eastern China, Southern
465 China and Central-West China), PM_{2.5} concentrations are largely
466 contributed by local emissions during the most polluted days compared
467 with normal days. In the future with emissions reductions for better air

[quality in China, decreasing air pollution should consider aerosols from both Chinese local emissions and pollutant transport from outside of China.](#)

Despite the large reductions in emissions, near-surface PM_{2.5} concentrations in the North China Plain and Eastern China increased a lot during the most polluted days of COVID-19 lockdown (with the highest daily PM_{2.5} concentration in February 2020), with the largest increases of more than 20 µg m⁻³. In addition to local emissions, regional transport of pollutants is also an important factor that causes haze events in China. The increases in PM_{2.5} concentrations during the most polluted days over the North China Plain and Eastern China are largely influenced by the stagnant air condition resulting from the anomalous high pressure system and weakening of winds, which lead to a reduced ventilation and aerosol accumulation in the North China Plain, together with an increase in aerosol inflow from regional transport. During the most polluted day in Southwestern China, ROW contributes over 50% of the PM_{2.5} concentration increase, with enhanced southwesterly winds that drive pollution transport from South and Southeast Asia. It indicates that regional transport and unfavorable meteorology need to be taken into consideration when controlling local emissions to improve air quality in the near future.

[To highlight the roles of regional and foreign transport, the differences between Covid and Baseline simulations in relative contributions to PM_{2.5} burden from local, region \(RCN\) and foreign \(ROW\) emissions are given](#)

490 in Figure S6. During the COVID-19 period, the local and RCN emission
491 contributions to PM_{2.5} were 1–4% lower than that in Base experiment over
492 NCP and NEC. In Eastern China, the contribution from the local emissions
493 decreased by 3–4% compared with Base experiment, while the
494 contribution from ROW increased by more than 5%. In Southern China,
495 50–70% of the PM_{2.5} burden is contributed by emissions from ROW in
496 Base experiment. During the COVID-19 period with low emission levels,
497 the contribution from ROW to PM_{2.5} burden in Southern China had an
498 increase of more than 5%. It indicates that the important role of
499 transboundary transport needs to be considered when controlling local
500 emissions to improve air quality in the near future.

501 Many studies have examined the importance of meteorology on
502 regional air quality during the COVID-19 lockdown period and
503 emphasized that, when meteorology is unfavorable, abrupt emissions
504 reductions cannot avoid severe air pollutions (Le et al. 2020; Sulaymon et
505 al. 2021; Shen et al. 2021). Through model simulations, Le et al. (2020)
506 found that abnormally high humidity promotes the heterogeneous
507 chemistry of aerosols, which have contributed to the increase of PM_{2.5} by
508 12% in northern China during the city lockdown period. Sulaymon et al.
509 (2021) found that significant increase in PM_{2.5} concentrations caused by
510 unfavorable meteorological conditions in Beijing-Tianjin-Hebei region
511 during the lockdown period based on Community Multiscale Air Quality

512 (CMAQ) model simulations. By analyzing the observational data and
513 model simulations, Shen et al. (2021) reported that 50% of the pollution
514 episodes during the COVID-19 lockdown in Hubei of China were due to
515 the stagnant meteorological conditions. Huang et al. (2020) found that the
516 stagnant air conditions and enhanced atmospheric oxidizing capacity
517 caused a severe haze event during the same time period. In line with
518 previous studies, we also revealed the stagnant air condition under the
519 anomalous high pressure system in the most polluted day over the North
520 China Plain. In addition to the meteorological conditions, the effect of
521 foreign transport was also raised in this study causing aerosol pollution in
522 southwestern China during COVID-19 outbreak.

523 There are a few uncertainties in this study. The CAM5 model has low
524 biases in reproducing the near-surface PM_{2.5} concentrations in China,
525 compared to observations, in part due to the incapability of simulating
526 some aerosol components of PM_{2.5} (e.g., ammonium and nitrate), excessive
527 aerosol wet removal during the long-range transport (Wang et al., 2013),
528 and uncertainties in observations. In majority of the climate models, the
529 simulation of nitrate and ammonium aerosols are not included in the
530 aerosol schemes, partly due to the complexity of calculation efficiency. For
531 example, in many of the CMIP6 models, only two of them provide nitrate
532 and ammonium mass mixing ratios. Many previous studies have evaluated
533 the global climate models performance in reproducing aerosol

534 concentrations (e.g., Fan et al., 2018; Shindell et al., 2013; Yang et al.,
535 2017a,b). In general, the models can well simulate aerosols in North
536 America and Europe but significantly underestimates aerosols in East Asia
537 by about -36 to -58 % compared with observations. It can lead to an
538 underestimation of aerosols contributed by Chinese local emissions in
539 magnitudes, but might not change the main conclusions of this study.

540 Uncertainties in the estimate of emission reductions in different source
541 regions during the COVID-19 pandemic can also introduce uncertainties
542 to our results. During the COVID-19 lockdown, greenhouse gas emissions
543 also decreased (Le Quéré et al., 2020), but the effect of greenhouse gas
544 reduction on meteorology that potentially influence aerosol distributions
545 was not taken into consideration. Nevertheless, this study is the first
546 attempt to provide source apportionment of aerosols in covering the whole
547 China during the COVID-19 outbreak, which is beneficial to the
548 investigation of policy implications for future air pollution control.

549 ***Data availability.***

550 The CAM5 model is available at
551 <http://www.cesm.ucar.edu/models/cesm1.2/> (last access: ~~25 October 2020~~
552 [August 2021](#)). CAM5-EAST model code and results can be made available
553 upon request. The surface PM_{2.5} observations are from the China National
554 Environmental Monitoring Center (CNEMC, <http://www.cnemc.cn>, last
555 access: ~~25 October 2020~~ [August 2021](#))

556 ***Competing interests.***

557 The authors declare that they have no conflict of interest.

558 ***Author contribution.***

559 YY and LR designed the research; YY performed the model simulations;
560 LR analyzed the data. All authors discussed the results and wrote the paper.

561 ***Acknowledgments.***

562 This study was supported by the National Key Research and Development
563 Program of China (grant 2020YFA0607803 [and 2019YFA0606800](#)) and
564 the National Natural Science Foundation of China (grant 41975159). HW
565 acknowledges the support by the U.S. Department of Energy (DOE),
566 Office of Science, Office of Biological and Environmental Research (BER).
567 The Pacific Northwest National Laboratory (PNNL) is operated for DOE
568 by the Battelle Memorial Institute under contract DE-AC05-76RLO1830.

569 **Reference**

570

571 Anderson, T.L., Charlson, R.J., Schwartz, S.E., Knutti, R., Boucher, O., Rodhe, H., Heintzenberg,
572 J.: Climate forcing by aerosol—a hazy picture, *Science*, 300, 1103-1104,
573 <https://doi.org/10.1126/science.1084777>, 2003.

574

575 Bao, R., Zhang, A.: Does lockdown reduce air pollution? Evidence from 44 cities in northern China,
576 ~~Science~~ ~~of~~ ~~The~~ ~~Total~~ ~~Environment~~ ~~Environ.~~, 731, 139052,
577 <https://doi.org/10.1016/j.scitotenv.2020.139052>, 2020.

578

579 Chai, F., Gao, J., Chen, Z., Wang, S., Zhang, Y., Zhang, J., Zhang, H., Yun, Y., Ren, C.: Spatial and
580 temporal variation of particulate matter and gaseous pollutants in 26 cities in China, ~~Journal of~~
581 ~~Environmental~~ ~~Environ.~~ ~~Sciences~~ ~~Sci.~~, 26, 75–82, [https://doi.org/10.1016/S1001-](https://doi.org/10.1016/S1001-0742(13)60383-6)
582 0742(13)60383-6, 2014.

583

584 China State Council: Action Plan on Prevention and Control of Air Pollution, China State Council,
585 Beijing, China, http://www.gov.cn/zwggk/2013-09/12/content_2486773.htm (last access: 27
586 September 2020), 2013.

587

588 Dong, E., Du, H., Gardner, L.: An interactive web-based dashboard to track COVID-19 in real time,
589 *Lancet Infectious—Infect. Diseases* ~~Dis.~~, 20, 533–534, [https://doi.org/10.1016/S1473-](https://doi.org/10.1016/S1473-3099(20)30120-1)
590 3099(20)30120-1, 2020.

591

592 Fan, H., Zhao, C., Yang, Y.: A comprehensive analysis of the spatio-temporal variation of urban air
593 pollution in China during 2014–2018, ~~Atmos. Environ.~~ ~~Atmospheric~~ ~~Environment~~, 220,
594 117066, <https://doi.org/10.1016/j.atmosenv.2019.117066>, 2020.

595

596 [Fan, T., Liu, X., Ma, P.-L., Zhang, Q., Li, Z., Jiang, Y., Zhang, F., Zhao, C., Yang, X., Wu, F., and](#)
597 [Wang, Y.: Emission or atmospheric processes? An attempt to attribute the source of large bias](#)
598 [of aerosols in eastern China simulated by global climate models, *Atmos. Chem. Phys.*, 18,](#)
599 [1395–1417, <https://doi.org/10.5194/acp-18-1395-2018>, 2018.](#)

600

601 Gelaro, R., McCarty, W., Suárez, M. J., Todling, R., Molod, A., Takacs, L., Randles, C. A.,
602 Darmenov, A., Bosilovich, M. G., Reichle, R., Wargan, K., Coy, L., Cullather, R., Draper, C.,
603 Akella, S., Buchard, V., Conaty, A., da Silva, A. M., Gu, W., Kim, G., Koster, R., Lucchesi, R.,
604 Merkova, D., Nielsen, J. E., Partyka, G., Pawson, S., Putman, W., Rienecker, M., Schubert, S.
605 D., Sienkiewicz, M., Zhao, B.: The Modern-Era Retrospective Analysis for Research and
606 Applications, Version 2 (MERRA-2), *J. Climate*, 30, 5419–5454, [https://doi.org/10.1175/JCLI-](https://doi.org/10.1175/JCLI-D-16-0758.1)
607 D-16-0758.1, 2017.

608

609 Hadley, O. L., Ramanathan, V., Carmichael, G. R., Tang, Y., Corrigan, C. E., Roberts, G. C., Mauget,
610 G. S.: Trans-Pacific transport of black carbon and fine aerosol ($D < 2.5\mu\text{m}$) into North America,
611 ~~J. Geophys. Res.~~ ~~Journal~~ ~~of~~ ~~Geophysical~~ ~~Research~~, 112, D05309,

612 <https://doi.org/10.1029/2006JD007632>, 2007.

613

614 Heft-Neal, S., Burney, J., Bendavid, E., Burke, M.: Robust relationship between air quality and
615 infant mortality in Africa, *Nature*, 559, 254. <https://doi.org/10.1038/s41586-018-0263-3>, 2018.

616

617 Hurrell, J. W., Holland, M. M., Gent, P. R., Ghan, S., Kay, J. E., Kushner, P. J., Lamarque, J. F.,
618 Large, W. G., Lawrence, D., Lindsay, K., Lipscomb, W. H., Long, M. C., Mahowald, N.,
619 Marsh, D. R., Neale, R. B., Rasch, P., Vavrus, S., Vertenstein, M., Bader, D., Collins, W. D.,
620 Hack, J. J., Kiehl, J., Marshall, S.: The Community Earth System Model A Framework for
621 Collaborative Research, *Bulletin Of The American Meteorological Society*,
622 94, 1339–1360, <https://doi.org/10.1175/BAMS-D-12-00121.1>, 2013.

623

624 Huang, X., Ding, A., Gao, J., Zheng, B., Zhou, D., Qi, X., Tang, R., Ren, C., Nie, W., Chi, X., Wang,
625 J., Xu, Z., Chen, L., Li, Y., Che, F., Pang, N., Wang, H., Tong, D., Qin, W., Cheng, W., Liu, W.,
626 Fu, Q., Chai, F., Davis, S. J., Zhang, Q., He, K.: Enhanced secondary pollution offset reduction
627 of primary emissions during COVID-19 lockdown in China, *National Science
628 Review*, nwaal37, <https://doi.org/10.1093/nsr/nwaa137>, 2020.

629

630 Kong, L., Feng, M., Liu, Y., Zhang, Y., Zhang, C., Li, C., Qu, Y., An, J., Liu, X., Tan, Q., Cheng, N.,
631 Deng, Y., Zhai, R., Wang, Z.: Elucidating the pollution characteristics of nitrate, sulfate and
632 ammonium in PM_{2.5} in Chengdu, southwest China, based on 3-year measurements, *Atmos.
633 Chem. Phys., Atmospheric Chemistry and Physics*, 20, 11181–11199,
634 <https://doi.org/10.5194/acp-20-11181-2020>, 2020.

635

636 Liao, H., Chang, W., Yang, Y.: Climatic effects of air pollutants over China: A review, *Advances in
637 Atmospheric Sciences*, 32, 115–139, <https://doi.org/10.1007/s00376-014-0013-x>,
638 2015.

639

640 Le, T., Wang, Y., Liu, L., Yang, J., Yung, Y. L., Li, G., Seinfeld, J. H.: Unexpected air pollution with
641 marked emission reductions during the COVID-19 outbreak in China, *Science*, 369, 702–706,
642 <https://doi.org/10.1126/science.abb7431>, 2020.

643

644 Le Quéré, C., Jackson, R. B., Jones, M. W., Smith, A. J. P., Abernethy, S., Andrew, R. M., De-Gol,
645 A. J., Willis, D. R., Shan, Y. L., Canadell, J. G., Friedlingstein, P., Felix Creutzig, F., Peters,
646 G., P.: Temporary reduction in daily global CO₂ emissions during the COVID-19 forced
647 confinement, *Nature Climate Change*, 10, 647–653,
648 <https://doi.org/10.1038/s41558-020-0797-x>, 2020.

649

650 Lelieveld, J., Klingmüller, K., Pozzer, A., Burnett, R. T., Haines, A., Ramanathan, V.: Effects of fossil
651 fuel and total anthropogenic emission removal on public health and climate. *P. Natl. Acad.
652 Sci. Proceedings of the National Academy of Sciences*, 116, 7192–7197,
653 <https://doi.org/10.1073/pnas.1819989116>, 2019.

654

655 Li, L., Li, Q., Huang, L., Wang, Q., Zhu, A., Xu, J., Liu, Z., Li, H., Shi, L., Li, R., Azari, M., Wang,

656 Y., Zhang, X., Liu, Z., Zhu, Y., Zhang, K., Xue, S., Ooi, M., C., G., Zhang, D., Chan, A.: Air
657 quality changes during the COVID-19 lockdown over the Yangtze River Delta Region: An
658 insight into the impact of human activity pattern changes on air pollution variation. *Science of
659 The Total Environment Environ.*, 732, 139282. <https://doi.org/10.1016/j.scitotenv.2020.139282>,
660 2020.

661

662 Liu, X., Easter, R. C., Ghan, S. J., Zaveri, R., Rasch, P., Shi, X., Lamarque, J., F., Gettelman, A.,
663 Morrison, H., Vitt, F., Conley, A., Park, S., Neale, R., Hannay, C., Ekman, A. M. L., Hess, P.,
664 Mahowald, N., Collins, W., Iacono, M. J., Bretherton, C. S., Flanner, M. G., Mitchell, D.:
665 Toward a minimal representation of aerosols in climate models: description and evaluation in
666 the Community Atmosphere Model CAM5, *Geoscientific Geosci. Model Development Dev.*, 5,
667 709–739. <https://doi.org/10.5194/gmd-5-709-2012>, 2012.

668

669 Liu, Y., Hong, Y., Fan, Q., Wang, X., Chan, P., Chen, X., Lai, A., Wang, M., Chen, X.: Source-
670 receptor relationships for PM_{2.5} during typical pollution episodes in the Pearl River Delta city
671 cluster, China, *Science of The Total Environment Environ.*, 596, 194-206,
672 <https://doi.org/10.1016/j.scitotenv.2017.03.255>, 2017.

673

674 [Lund, M. T., Myhre, G., and Samset, B. H.: Anthropogenic aerosol forcing under the Shared
675 Socioeconomic Pathways, *Atmos. Chem. Phys.*, 19, 13827–13839,
676 <https://doi.org/10.5194/acp-19-13827-2019>, 2019.](#)

677

678 [Lyakaremye, V., Zeng, G., Siebert, A., Yang, X.: Contribution of external forcings to the observed
679 trend in surface temperature over Africa during 1901–2014 and its future projection from
680 CMIP6 simulations, *Atmos. Res.*, 254, 105512,
681 <https://doi.org/10.1016/j.atmosres.2021.105512>, 2021.](#)

682

683 Ramanathan, V. C. P. J., Crutzen, P. J., Kiehl, J. T., Rosenfeld, D.: Aerosols, climate, and the
684 hydrological cycle, *science*, 294, 2119-2124, <https://doi.org/10.1126/science.1064034>, 2001.

685

686 Ren, L., Yang, Y., Wang, H., Zhang, R., Wang, P., Liao, H.: Source attribution of Arctic aerosols and
687 associated Arctic warming trend during 1980–2018, *Atmos. Chem. Phys., Atmospheric
688 Chemistry and Physics*, 20, 9067-9085, <https://doi.org/10.5194/acp-2020-3,2020>.

689

690 Sharma, S., Zhang, M., Anshika, Gao, J., Kota, S. H.: Effect of restricted emissions during covid-
691 19 on air quality in india, *Science of The Total Environment Environ.*, 728, 138878,
692 <https://doi.org/10.1016/j.scitotenv.2020.138878>, 2020.

693

694 [Shen, L., Zhao, T., Wang, H., Liu, J., Bai, Y., Kong, S., Zheng, H., Zhu, Y., Shu, Z.: Importance of
695 meteorology in air pollution events during the city lockdown for COVID-19 in Hubei Province,
696 Central China, *Sci. Total Environ.*, 754, 142227,
697 <https://doi.org/10.1016/j.scitotenv.2020.142227>, 2021.](#)

698

699 [Shindell, D. T., Lamarque, J.-F., Schulz, M., Flanner, M., Jiao, C., Chin, M., Young, P. J., Lee, Y.](#)

700 [H., Rotstayn, L., Mahowald, N., Milly, G., Faluvegi, G., Balkanski, Y., Collins, W. J., Conley,](#)
701 [A. J., Dalsoren, S., Easter, R., Ghan, S., Horowitz, L., Liu, X., Myhre, G., Nagashima, T., Naik,](#)
702 [V., Rumbold, S. T., Skeie, R., Sudo, K., Szopa, S., Takemura, T., Voulgarakis, A., Yoon, J.-H.,](#)
703 [and Lo, F.: Radiative forcing in the ACCMIP historical and future climate simulations, *Atmos.*](#)
704 [*Chem. Phys.*, 13, 2939–2974, <https://doi.org/10.5194/acp-13-2939-2013>, 2013.](#)
705
706 Smith, C. J., Kramer, R. J., Myhre, G., Alterskjær, K., Collins, W., Sima, A., Boucher, O., Dufresne,
707 J.-L., Nabat, P., Michou, M., Yukimoto, S., Cole, J., Paynter, D., Shiogama, H., O'Connor, F.
708 M., Robertson, E., Wiltshire, A., Andrews, T., Hannay, C., Miller, R., Nazarenko, L., Kirkevåg,
709 A., Olivie, D., Fiedler, S., Lewinschal, A., Mackallah, C., Dix, M., Pincus, R., Forster, P. M.:
710 Effective radiative forcing and adjustments in CMIP6 models, [Atmos. Chem.](#)
711 [Phys., Atmospheric Chemistry and Physics](#), 20, 9591–9618, [https://doi.org/10.5194/acp-20-](https://doi.org/10.5194/acp-20-9591-2020)
712 [9591-2020](https://doi.org/10.5194/acp-20-9591-2020), 2020.
713
714 [Sulaymon, I. D., Zhang, Y., Hopke, P. K., Hu, J., Zhang, Y., Li, L., Mei, X., Gong, K., Shi, Z., Zhao,](#)
715 [B., Zhao, F.: Persistent high PM_{2.5} pollution driven by unfavorable meteorological conditions](#)
716 [during the COVID-19 lockdown period in the Beijing-Tianjin-Hebei region, China, *Environ.*](#)
717 [Res., 198, 111186, <https://doi.org/10.1016/j.envres.2021.111186>, 2021.
718
719 Tian, H., Liu, Y., Li, Y., Wu, C., Chen, B., Kraemer, M.U.G., Li, B., Cai, J., Xu, B., Yang, Q., Wang,
720 B., Yang, P., Cui, Y., Song, Y., Zheng, P., Wang, Q., Bjornstad, O.N., Yang, R., Grenfell, B.T.,
721 Pybus, O.G., Dye, C.: An investigation of transmission control measures during the first 50
722 days of the COVID-19 epidemic in China, *Science*, b6105
723 <https://doi.org/10.1126/science.abb6105>, 2020.
724
725 Vautard, R., Yiou, P., Oldenborgh, G.: Decline of fog, mist and haze in Europe over the past 30 years,
726 \[Nature Nat. Geoscience Geosci.\]\(#\), 2, 115–119, <https://doi.org/10.1038/ngeo414>, 2009.
727
728 Wang, H., Easter, R. C., Rasch, P. J., Wang, M., Liu, X., Ghan, S. J., Qian, Y., Yoon, J.-H., Ma, P.-
729 L., Vinoj, V.: Sensitivity of remote aerosol distributions to representation of cloud–aerosol
730 interactions in a global climate model, \[Geoscientific Geosci. Model Development Dev.\]\(#\), 6, 765–
731 782, <https://doi.org/10.5194/gmd-6-765-2013>, 2013.
732
733 Wang, H., Rasch, P. J., Easter, R. C., Singh, B., Zhang, R., Ma, P. L., Qian, Y., Ghan, S. J., Beagley,
734 N.: Using an explicit emission tagging method in global modeling of source-receptor
735 relationships for black carbon in the Arctic: Variations, sources, and transport pathways,
736 \[Journal of Geophysical Research Res.\]\(#\), 119, 12888–12909,
737 <https://doi.org/10.1002/2014JD022297>, 2014.
738
739 Wang, H., Easter, R. C., Zhang, R., Ma, P., Singh, B., Zhang, K., Ganguly, D., Rasch, P. J., Burrows,
740 S. M., Ghan, S. J., Lou, S., Qian, Y., Yang, Y., Feng, Y., Flanner, M., Leung, L. R., Liu, X.,
741 Shrivastava, M., Sun, J., Tang, Q., Xie, S., Yoon, J.: Aerosols in the E3SM Version 1: New
742 Developments and Their Impacts on Radiative Forcing, \[Journal of Advances in Modeling\]\(#\)
743 \[Model. Earth Systems Sy.\]\(#\), 12, 293, <https://doi.org/10.1029/2019MS001851>, 2020.](#)

744

745 Wang, P., Chen, K., Zhu, S., Wang, P., Zhang, H.: Severe air pollution events not avoided by reduced
746 anthropogenic activities during COVID-19 outbreak, Resources-Resour. Conservation-Conserv.
747 and RecyclingRecycl., 158, 104814, <https://doi.org/10.1016/j.resconrec.2020.104814>, 2020.

748

749 Wang, Q., Huang, R. J., Cao, J., Tie, X., Shen, Z., Zhao, S., Han, Y., Li, G., Li, Z., Ni, H., Zhou, Y.,
750 Wang, M., Chen, Y., Zhou, Y.: Contribution of regional transport to the black carbon aerosol
751 during winter haze period in Beijing, Atmospheric-Atmos. EnvironmentEnviron., 132,11-28,
752 <https://doi.org/10.1016/j.atmosenv.2016.02.031>, 2016.

753

754 Watson, J. G.: Visibility: Science and regulation. Journal of the Air and Waste Management Manage.
755 AssociationAssoc., 52, 628-713, <https://doi.org/10.1080/10473289.2002.10470813>, 2002.

756

757 Xu, Q., Wang, S., Jiang, J., Bhattarai, N., Li, X., Chang, X., Qiu, X., Zheng, M., Hua, Y., Hao, J.:
758 Nitrate dominates the chemical composition of PM_{2.5} during haze event in Beijing, China, The
759 Science of the Total EnvironmentEnviron., 689, 1293–1303.
760 <https://doi.org/10.1016/j.scitotenv.2019.06.294>, 2019.

761

762 Xue, W. B., Fu, F., Wang, J. N., Tang, G. Q., Lei, Y., Yang, J. T., Wang, Y. S.: Numerical study on
763 the characteristics of regional transport of PM_{2.5} in China, Journal of Environmental Environ.
764 Sciences China, 34, 1361–1368, 2014.

765

766 Yang, Y., Wang, H., Smith, S. J., Ma, P. L., Rasch, P. J.: Source attribution of black carbon and its
767 direct radiative forcing in China, Atmospheric Atmos. Chemistry and PhysiesPhys., 17, 4319–
768 4336, <https://doi.org/10.5194/acp-17-4319-2017>, 2017a.

769

770 Yang, Y., Wang, H., Smith, S. J., Easter, R., Ma, P. L., Qian, Y., Yu, H., Li, C., Rasch, P. J.: Global
771 source attribution of sulfate concentration and direct and indirect radiative forcing,
772 Atmospheric Atmos. Chemistry and PhysiesPhys., 17, 8903–8922,
773 <https://doi.org/10.5194/acp-17-8903-2017>, 2017b.

774

775 Yang, Y., Wang, H., Smith, S. J., Zhang, R., Lou, S., Qian, Y., Ma, P.-L., Rasch, P. J.: Recent
776 intensification of winter haze in China linked to foreign emissions and meteorology, Sci.
777 Rep.Scientific Reports, 8, 2107, <https://doi.org/10.1038/s41598-018-20437-7>, 2018a.

778

779 Yang, Y., Wang, H., Smith, S. J., Easter, R. C., Rasch, P. J.: Sulfate aerosol in the Arctic: Source
780 attribution and radiative forcing, J. Geophys. Res.,Journal of Geophysical Research:
781 Atmospheres, 123, 1899–1918, <https://doi.org/10.1002/2017JD027298>, 2018b.

782

783 Yang, Y., Wang, H., Smith, S. J., Zhang, R., Lou, S., Yu, H., Li, C., Rasch, P. J.: Source
784 apportionments of aerosols and their direct radiative forcing and long-term trends over
785 continental United States, Earth's Future, 6, 793–808, <https://doi.org/10.1029/2018EF000859>,
786 2018c.

787

788 Yang, Y., Smith, S. J., Wang, H., Lou, S., Rasch, P. J.: Impact of anthropogenic emission injection
789 height uncertainty on global sulfur dioxide and aerosol distribution, ~~J. Geophys. Res., Journal~~
790 ~~of Geophysical Research: Atmospheres,~~ 124, 4812–4826,
791 <https://doi.org/10.1029/2018JD030001>, 2019a.

792

793 Yang, Y., Smith, S. J., Wang, H., Mills, C. M., Rasch, P. J.: Variability, timescales, and nonlinearity
794 in climate responses to black carbon emissions, ~~Atmospheric Atmos. Chemistry and~~
795 ~~Physics Phys.~~, 19, 2405–2420, <https://doi.org/10.5194/acp-19-2405-2019>, 2019b.

796

797 Yang, Y., Lou, S., Wang, H., Wang, P., Liao, H.: Trends and source apportionment of aerosols in
798 Europe during 1980–2018, ~~Atmospheric Atmos. Chemistry and Physics Phys.~~, 20, 2579–2590,
799 <https://doi.org/10.5194/acp-20-2579-2020>, 2020.

800

801 Yu, H. B., Remer, L. A., Chin, M., Bian, H. S., Tan, Q., Yuan, T. L., Zhang, Y.: Aerosols from
802 overseas rival domestic emissions over North America, *Science*, 337, 566–569,
803 <https://doi.org/10.1126/science.1217576>, 2012.

804

805 Yu, H., Remer, L. A., Chin, M., Bian, H., Kleidman, R. G., Diehl, T.: A satellite-based assessment
806 of transpacific transport of pollution aerosol, ~~J. Geophys. Res., Journal of Geophysical~~
807 ~~Research,~~ 113, D14S12, <https://doi.org/10.1029/2007JD009349>, 2008.

808

809 Zhang, R., Wang, H., Hegg, D. A., Qian, Y., Doherty, S. J., Dang, C., Ma, P. L., Rasch, P. J., Fu, Q.:
810 Quantifying sources of black carbon in western North America using observationally based
811 analysis and an emission tagging technique in the Community Atmosphere Model,
812 ~~Atmospheric Atmos. Chemistry and Physics Phys.~~, 15, 12,805–12,822,
813 <https://doi.org/10.5194/acpd-15-12957-2015>, 2015.

814

815 Zheng, B., Tong, D., Li, M., Liu, F., Hong, C., Geng, G., Li, H., Li, X., Peng, L., Qi, J., Yan, L.,
816 Zhang, Y., Zhao, H., Zheng, Y., He, K., Zhang, Q.: Trends in China's anthropogenic emissions
817 since 2010 as the consequence of clean air actions, ~~Atmospheric Atmos. Chemistry and~~
818 ~~Physics Phys.s~~, 18, 14095–14111, <https://doi.org/10.5194/acp-18-14095-2018>, 2018.

819

820 [Zhuang, B. L., Li, S., Wang, T. J., Liu, J., Chen, H. M., Chen, P. L., Li, M. M., Xie, M.: Interaction](#)
821 [between the Black Carbon Aerosol Warming Effect and East Asian Monsoon Using RegCM4,](#)
822 [J. Climate, 31, 9367-9388, https://doi.org/10.1175/JCLI-D-17-0767.1, 2018.](#)

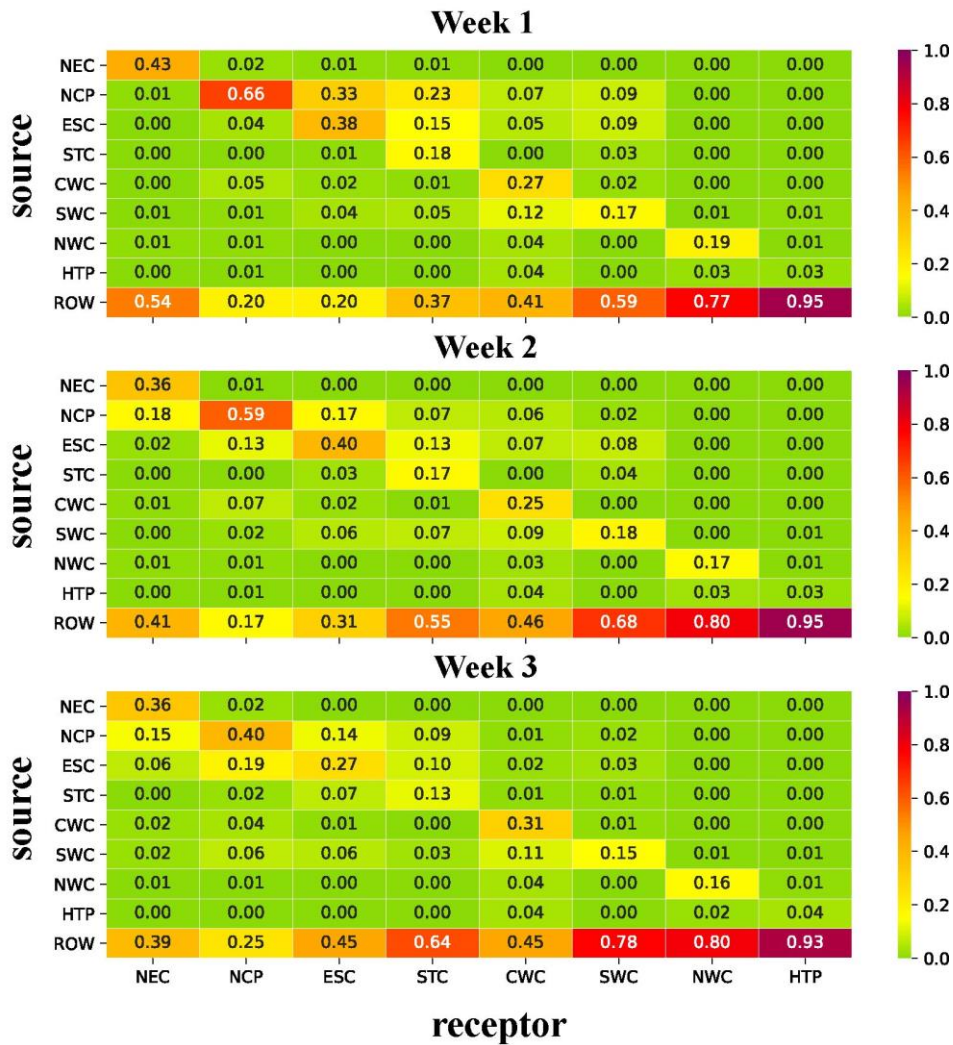
823

824 [Zhu, J., Xia, X., Che, H., Wang, J., Zhang, J., Duan, Y.: Study of aerosol optical properties at](#)
825 [Kunming in southwest China and longrange transport of biomass burning aerosols from North](#)
826 [Burma, Atmos. Res., 169, 237–247, https://doi.org/10.1016/j.atmosres.2015.10.012, 2016.](#)

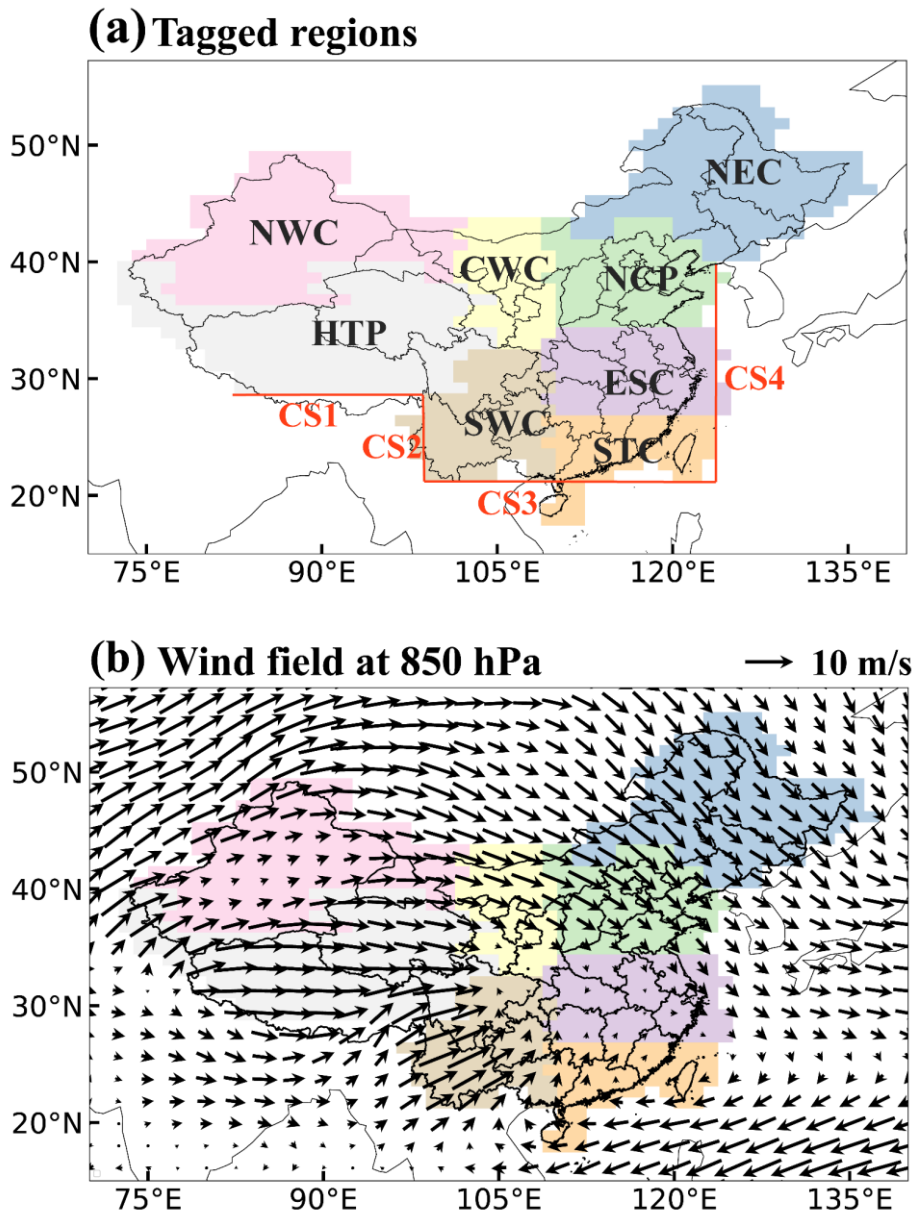
827

828 [Zhu, J., Xia, X., Wang, J., Zhang, J., Wiedinmyer, C., Fisher, J. A., Keller, C. A.: Impact of Southeast](#)
829 [Asian smoke on aerosol properties in Southwest China: First comparison of model simulations](#)
830 [with satellite and ground observations, J. Geophys. Res. Atmos., 122, 3904–3919,](#)
831 <https://doi.org/10.1002/2016JD025793>, 2017.

832 **Table 1.** Fractional contributions of emissions from nine tagged source regions (vertical
 833 axis) to mean PM_{2.5} column burden in eight receptor regions (horizontal axis) during
 834 the three time periods- ('Week 1': January 30–February 5, 'Week 2': February 6–
 835 February 12 and 'Week 3': February 13–February 19).
 836



837
 838



839

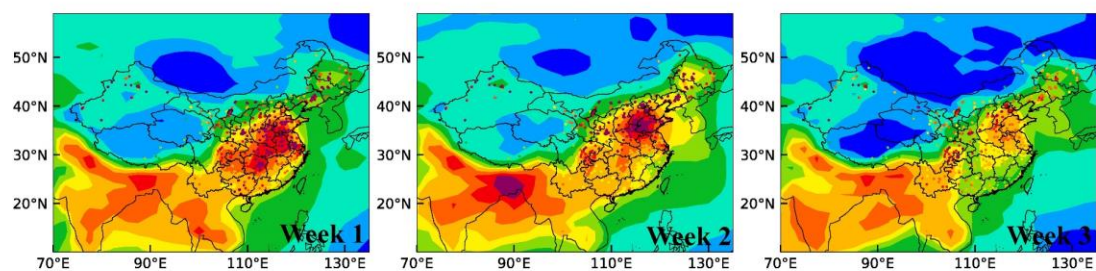
840

841 **Figure 1.** (a) Tagged source regions (NEC: Northeastern China, NCP: North China
 842 Plain, ESC: Eastern China, STC: Southern China, CWC: Central-West China, SWC:
 843 Southwestern China, NWC: Northwestern China, HTP: Himalayas and Tibetan Plateau,
 844 ROW: rest of the world) and (b) mean wind field (units: m s^{-1} , vectors) at 850 hPa
 845 during the [time period of interest: three weeks of the study from January 30 to February](#)
 846 [19, which had the largest number of newly-diagnosed COVID-19 cases](#). Lines in (a)
 847 mark the cross-sections (CS) defined to study the transport of aerosols to and from
 848 China.

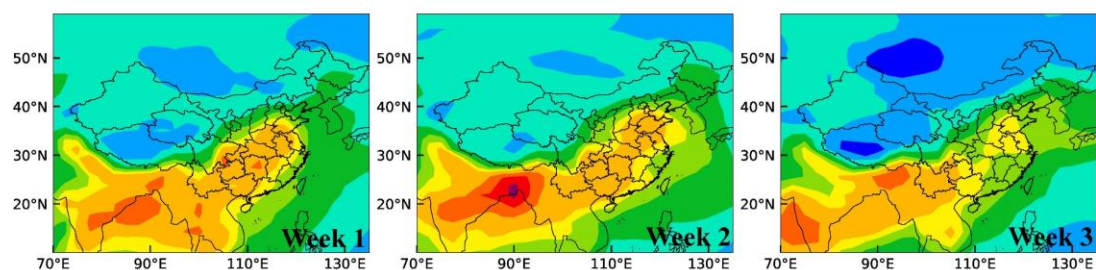
849

850

(a) PM_{2.5} surface conc. ($\mu\text{g m}^{-3}$)



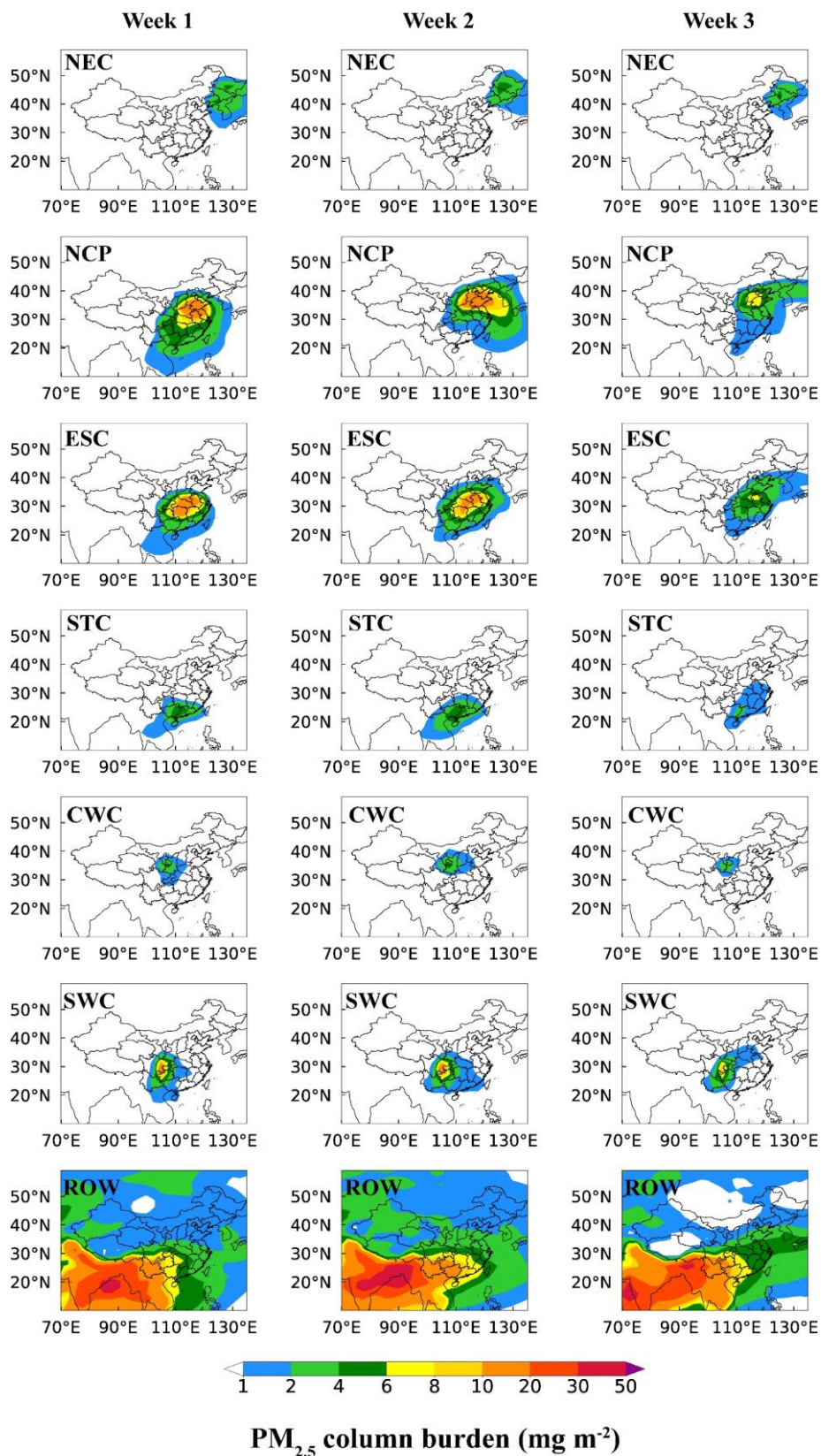
(b) PM_{2.5} column burden (mg m^{-2})



851

852

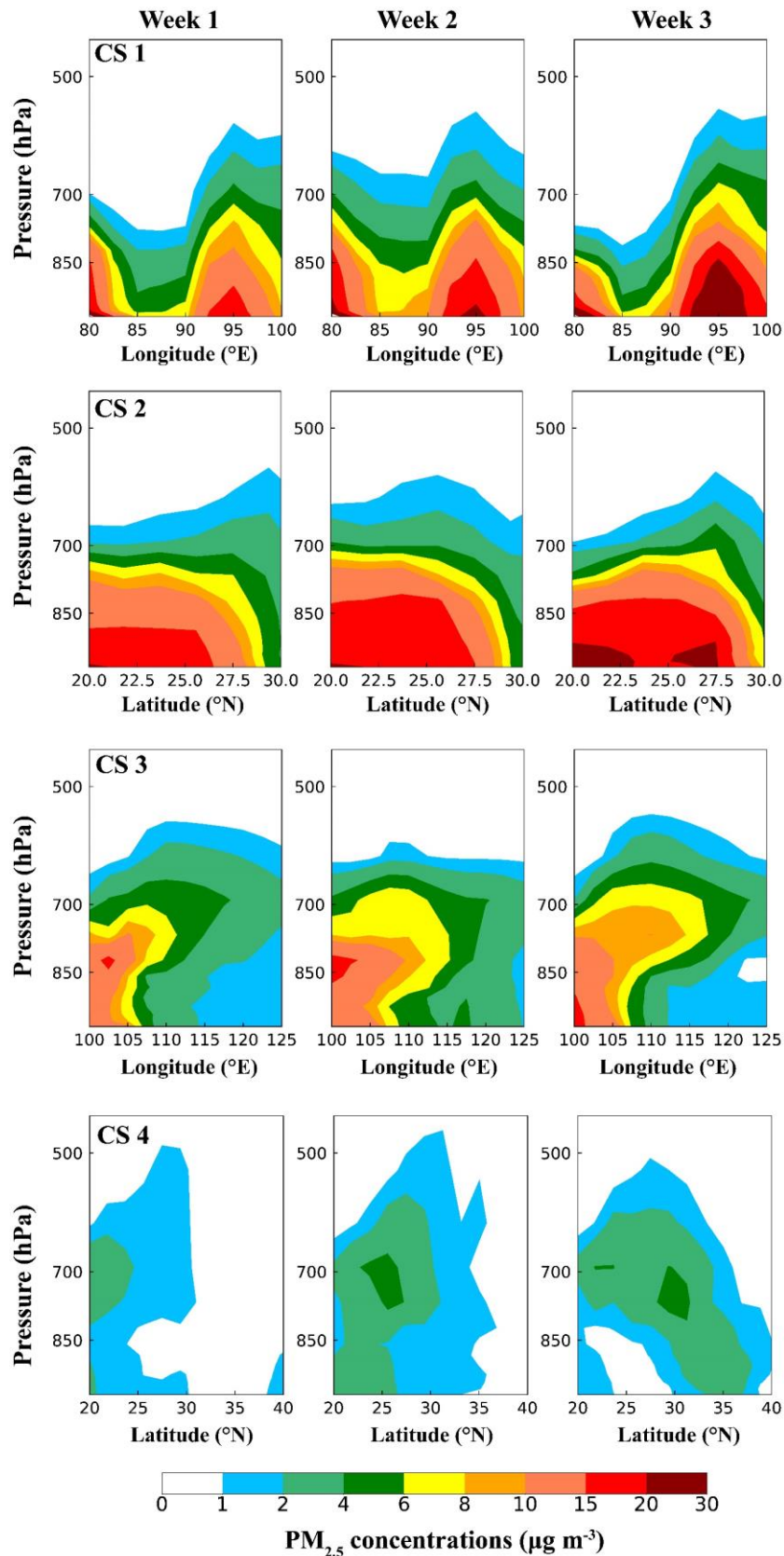
853 **Figure 2.** Spatial distribution of (a) the simulated and observed mean near-surface
854 PM_{2.5} concentrations ($\mu\text{g m}^{-3}$) and (b) PM_{2.5} column burden (mg m^{-2}) during January
855 30–February 5 (Week 1), February 6–February 12 (Week 2) and February 13–February
856 19 (Week 3).



857

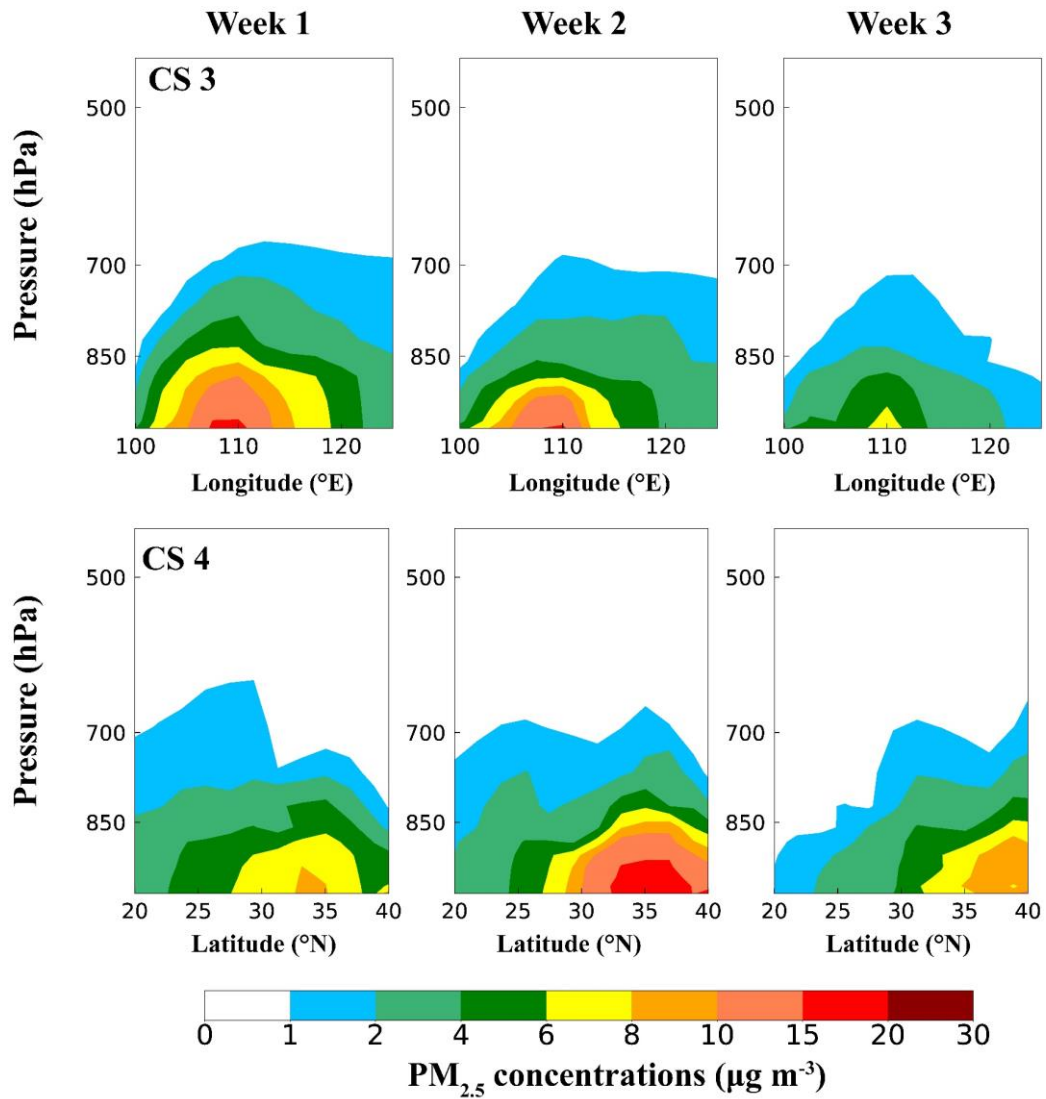
858 **Figure 43.** Spatial distribution of PM_{2.5} column burden (mg m⁻²) originating from the
 859 six major source regions in China (NEC, NCP, ESC, STC, CWC and SWC) and sources
 860 outside China (ROW) during the three time periods.

861



862

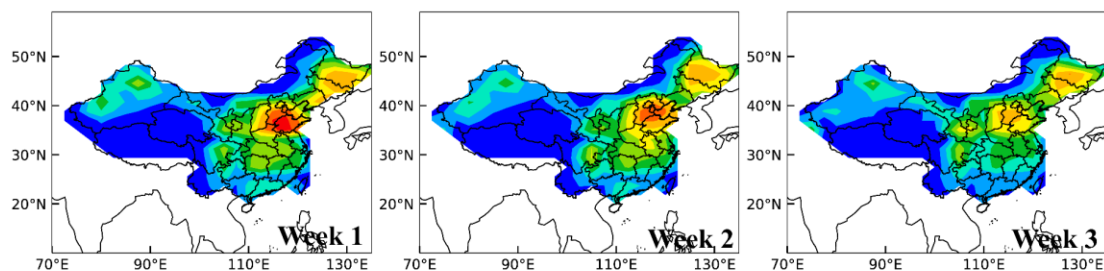
863 **Figure 54.** Vertical distributions of PM_{2.5} concentrations (µg m⁻³), originating from
 864 emissions outside China (i.e., ROW sources), across the latitudinal and/or longitudinal
 865 extents marked in Fig.1, respectively, during the three time periods.



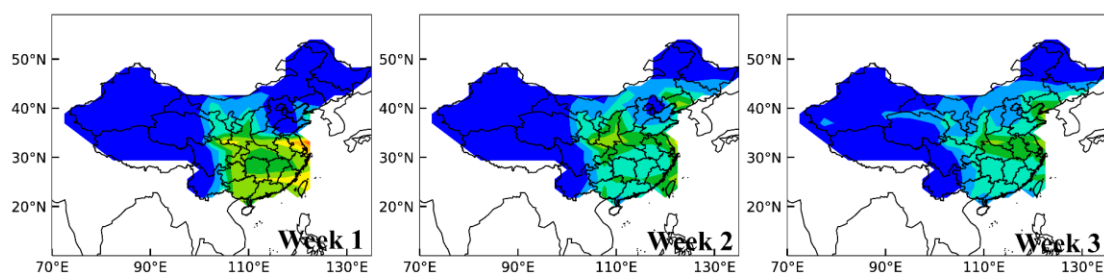
866
 867
 868
 869
 870
 871
 872
 873

Figure 65. Vertical distributions of PM_{2.5} concentrations (µg m⁻³), originating from domestic emissions in China, across the latitudinal and/or longitudinal extents marked in Fig.1, respectively, during the three time periods. The values along CS 1 and CS 2 are negligibly small.

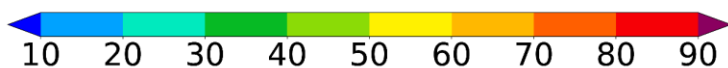
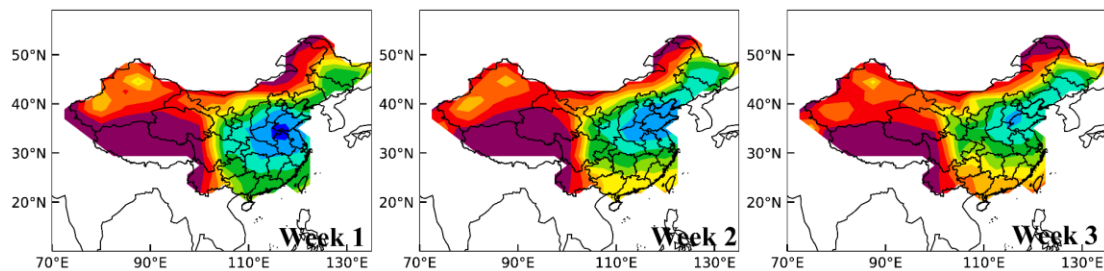
(a) Local contribution



(b) RCN contribution



(c) ROW contribution



Relative contribution to PM_{2.5} column burden (%)

874

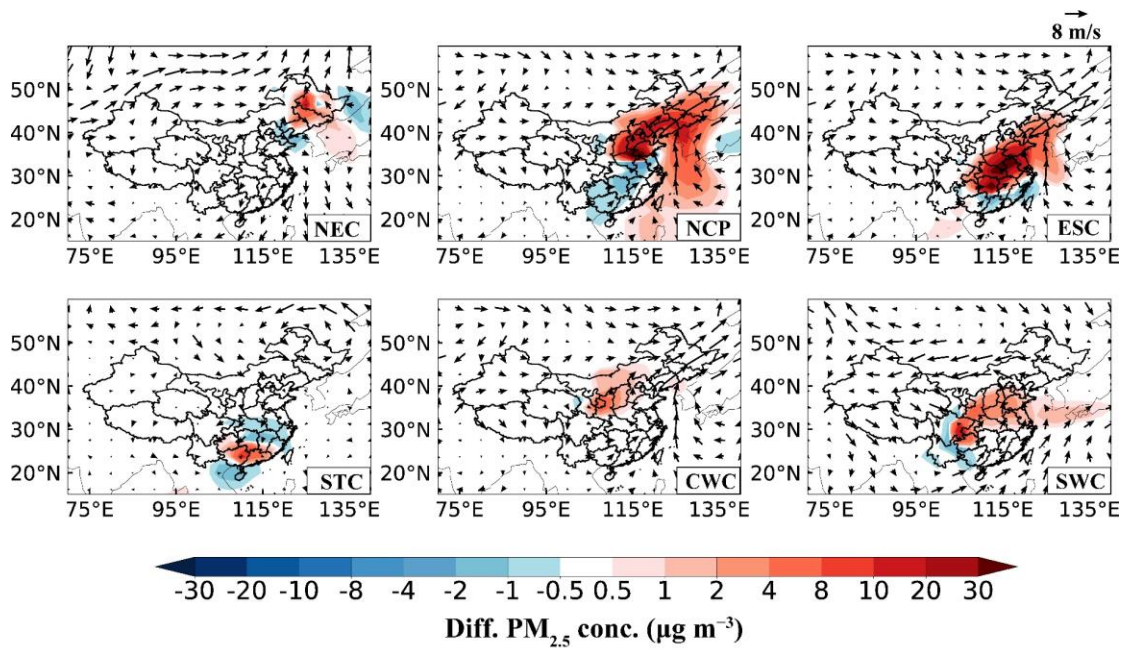
875

876

Figure 76. Relative contributions (%) of (a) local emissions, (b) the emissions from the rest of China (RCN) and (c) all sources outside China (rest of the world, ROW) to PM_{2.5} column burden during the three time periods.

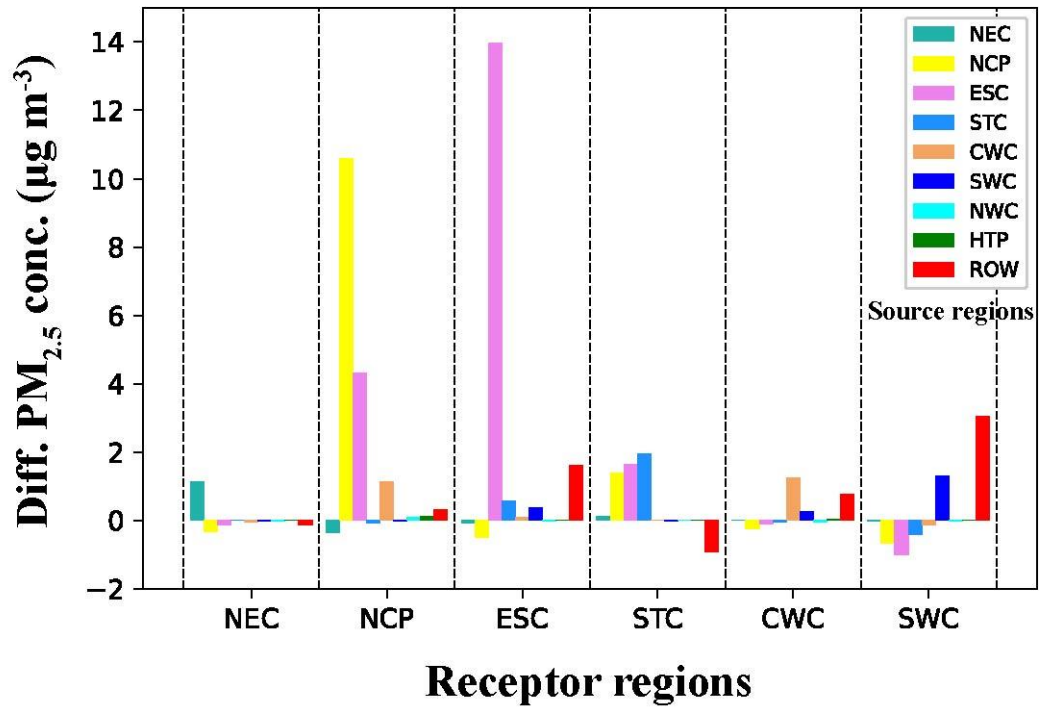
878

879



880
 881
 882
 883
 884
 885
 886

Figure 87. Composite differences in winds at 850 hPa (m s^{-1}) and near-surface $\text{PM}_{2.5}$ concentrations ($\mu\text{g m}^{-3}$) between the most polluted and normal days in February 2020. The most polluted day is defined as the day with the highest daily $\text{PM}_{2.5}$ concentration in February 2020 in each receptor region in China.



887

888

889 **Figure 98.** Composite differences in near-surface PM_{2.5} concentrations (µg m⁻³)
 890 averaged over receptor regions (marked on the horizontal axis) in China between [the](#)
 891 [most](#) polluted and normal days in February 2020 originating from individual source
 892 regions (corresponding color bars in each column).